Wave Motion

A multi-approach analysis for monitoring wave energy driven by coastal extremes

--Manuscript Draft--

Manuscript Number:	WAMOT-D-24-00009
Article Type:	Review Article
Section/Category:	Water waves
Keywords:	Extreme waves; Wave energy; physical modeling; Signal processing; MLP model
Corresponding Author:	NIZAR ABCHA Continental and Coastal Morphodynamics FRANCE
First Author:	Reine MATAR
Order of Authors:	Reine MATAR
	NIZAR ABCHA
	Iskander ABROUG
	Nicolas LECOQ
	Emma-Imen TURKI
Abstract:	This research investigates the behavior of extreme waves and the evolution of their frequencies in shallow waters and coastal areas. Laboratory experiments were conducted in a wave flume, deploying various wave spectra, including JONSWAP and Pierson-Moskowitz. These spectral waves were generated using the dispersive focusing technique. Fifty-one wave gauges facilitated comprehensive monitoring of wave characteristics and their propagation along the flume. This monitoring has been explored by applying power spectral density analysis to examine the subtleties of wave energy. Moreover, a spectral approach of discrete wavelets has been used to identify the frequency components of extreme waves and their complex evolution along the wave flume. The energy of the dominant frequency components, has experienced a significant decrease. Conversely, the energy of the remaining components has increased.The study highlights the repeatable and precise nature of results regarding the energy of the frequency components with good accuracy using the machine learning algorithm.

Dear Editor of the Wave Motion,

Enclosed is a paper, entitled “A multi-approach analysis for monitoring wave energy driven by coastal extremes” by Reine MATAR, Nizar ABCHA, Iskander ABROUG, Nicolas LECOQ, Emma-Imen TURKI

Please accept it as a candidate for publication in the Wave Motion.

This paper is our original unpublished work and it has not been submitted to any other journal for reviews.

Highlights

- The propagation of focused wave groups in intermediate water depth and the shoaling zone is studied
- The energy dissipation has increased with the nonlinearity S_0.
- Dominant frequency components lost energy, while the remaining components gained energy.
- Energy can be transferred between different frequency components.
- The predictions made using the MLP algorithm align well with the experimental data.

A multi-approach analysis for monitoring wave energy driven by coastal extremes

Reine MATAR[1], Nizar ABCHA[1*], Iskander ABROUG[1], Nicolas LECOQ[2], Emma-Imen TURKI[2]

[1]Normandy University, UNICAEN, UNIROUEN, CNRS, UMR 6143 M2C, 14000 Caen, France

[2]Normandy University, UNIROUEN, UNICAEN, CNRS, UMR 6143 M2C, 76000 Rouen, France

Abstract:

This research investigates the behavior of extreme waves and the evolution of their frequencies in shallow waters and coastal areas by coupling different approaches of physical modeling, spectral analysis, and Artificial Intelligence techniques. Laboratory experiments were conducted in a wave flume, deploying various wave spectra, including JONSWAP ($\gamma = 7$), JONSWAP ($\gamma = 3.3$), and Pierson-Moskowitz, covering a broad range of wave amplitudes. These spectral waves were generated using the dispersive focusing technique. Fifty-one wave gauges positioned at distances ranging from 4 m to 14 m from the wave generator facilitated comprehensive monitoring of wave characteristics and their propagation along the wave flume. This monitoring has been explored by applying power spectral density (PSD) analysis to examine the subtleties of wave energy. Moreover, a spectral approach of discrete wavelets has been used to identify the frequency components of extreme waves and their complex evolution along the wave flume. The energy of the dominant frequency components, d5 and d4, representing the peak frequency ($f_p = 0.75$ Hz) and its first harmonic ($2f_p = 1.5$ Hz), respectively, has experienced a significant decrease in energy. Conversely, the energy of the remaining components has increased. Results highlighted potential correlations between the dissipation of dominant frequency components and zones of higher energy dissipation. The study highlights the repeatable and precise nature of results regarding the energy of the frequency components with good accuracy using the Multilayer Perceptron (MLP) machine learning algorithm. The finding, emphasized in this work, has proven that employing a multi-approach analysis is crucial for monitoring wave energy driven by extreme coastal waves.

Keywords: *Extreme waves; Wave energy; Physical modeling; Signal processing; MLP model*

1. Introduction

Nowadays, chronic coastal hazards, including wave-driven flooding and erosion, are increasing in frequency and severity due to induced sea-level rise (SLR) and modified storminess patterns in the global context of climate change [1], [2]. Their impacts are also influenced by internal system characteristics such as geometry, topography slope, and sediment texture. These impacts are generally manifested through a series of changes, including coastal mechanisms and extensive economic and social costs [3], [4]. Extreme waves are typically generated in open seas during energetic storms and exhibit a spatiotemporal spectrum in nearshore zones. Their frequencies are modulated in areas of reduced depths such as surf zones. Therefore, characterizing nearshore wave behavior is key for reliable predictions of sediment transport, shoreline evolution, and future coastal management, including maritime structures and marine energy devices. The response of coastal zones to extreme events has been studied in previous works using observational methods, such as space and airborne techniques, numerical modeling, and laboratory experiments.

The physical characterization provided by the latter approach is essential in engineering solutions for coastal issues. Extensive research has been performed on wave characteristics in wave flumes [5]. Complicated physical processes, such as wave breaking, nonlinear wave-wave interactions, and energy transfer, are involved in the propagation of these extreme events in the form of steep wave trains [6], [7].

At the laboratory scale, various methods exist for generating extreme waves as discussed in [8]–[10]. Only the dispersive focusing mechanism for extreme wave generation [10] is considered in this paper. By combining several analytical techniques, the present study aims to gain insight into the relationships between wave behavior and energy dissipation.

In the literature, extreme waves are defined as large water waves with a crest-to-trough wave height H that exceeds twice the significant wave height H_s of the wave field [11], [12]. The experimental results demonstrate a relationship between a water depth drop and an increase in the probability of extreme waves [13], [14]. In ocean engineering, the wavelet analysis technique has been employed to explore the spectral components of non-stationary oceanographic drivers, such as waves and storm surges [15]. This method has been employed to discern wave groups with varying bathymetry [16], thereby predicting the occurrence of extreme events. While the Fourier

Transform analysis provides information about the frequency content of a signal over its entire duration, wavelet transforms offer time-frequency localization.

According to the existing literature, prior studies have often relied on short-duration signals, resulting in insufficient consideration of the temporal aspects of extreme events. Additionally, a limited application of wavelet transforms in coastal studies has been noticed. In particular, the Maximal Overlap Discrete Wavelet Transform (MODWT) is well-suited for detecting and analyzing intricate frequency components within coastal signals [17], [18]. Despite its potential, this method has not been widely adopted in the current research methodologies.

The objectives of this work are delineated as follows: (1) monitoring wave energy content using power spectral density analysis which provides a thorough comprehension of energy distribution across various frequencies in the wave spectrum. This allows the analysis of energy dissipation in shallow waters while varying the extreme events duration. And (2) identifying inherent frequency components and their assigned energy using the MODWT method. These aforementioned objectives will be fulfilled by the use of different approaches of physical modeling, spectral analysis, and artificial intelligence techniques. The coupling between different approaches will be useful to enhance our understanding of the energy behavior with its different frequency components along the shallow water environments.

This paper is organized into several sections. In section 2, the experimental setup and the tested wave conditions are introduced. The monitoring of wave energy behavior extracted from the power spectral density is outlined in Section 3. In Section 4, the frequency components study is presented. Finally, Section 5 concludes with the paper's findings, along with an overview of a learning algorithm application.

2. Experimental Set-Up

All experiments were performed at the wave flume in the Continental and Coastal Morphodynamics laboratory in Caen. This flume's length is 20 m, the width is 0.8 m, and the useful height ranges from 25 cm to 40 cm. To simulate different wave conditions, a piston-type wave generator from Edinburgh Designs Ltd is used.

Three wave spectra were chosen, including JONSWAP ($\gamma = 7$), JONSWAP ($\gamma = 3.3$), and Pierson-Moskowitz covering a wide range of amplitudes. The reference wave gauge (WG_R) signals for the three spectra mentioned earlier, using various numbers of wave trains are shown in Figure 2. To account for the varying duration of extreme events, one, three, six, and nine wave trains were generated, see Figure 2. Wave gauges positioned between 4m and 14m from the wave generator were used to measure the free surface elevation with a sampling rate of 32 Hz. Table 1 presents a summary of the parameters used.

The experimental configuration included two distinct sections: (1) A flat glass bottom, providing a hydraulically smooth surface, the water depth h_0 within this section was set at 0.3 meters. (2) An inclined PVC Slope positioned at a distance of 9.5 meters from the wave generator, the slope angle β was defined as 1/25 [19], corresponding to a slope gradient that enables wave transformation.

As shown in Figure 1, WG_R refers to the reference wave gauge located 4 meters away from the wave generator. To cover the 10-meter experimental area, five wave gauges were strategically placed 20 centimeters apart [20]. This arrangement was replicated ten times. Wave breaking was imposed at 2m from the slope's toe.

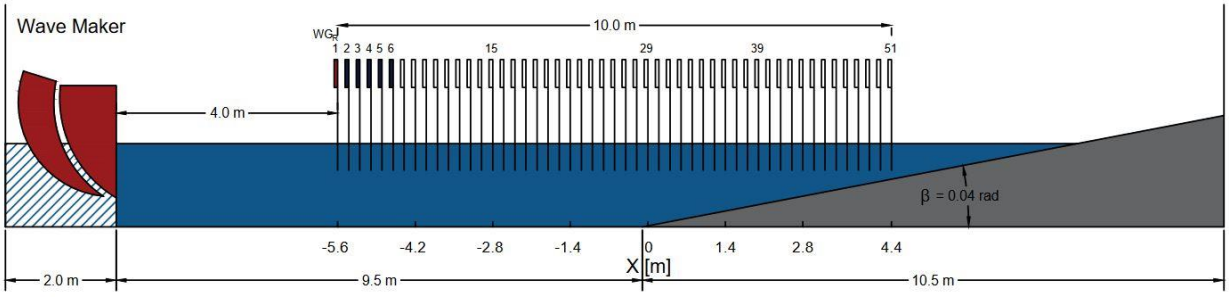

Figure 1. Sketch of the wave flume. The direction of propagation: from left to right.

The present focused wave groups use the linear NewWave profile [21], [22] as input. Each wave train consists of n sinusoidal wave components that phase together at a single point in time and space. The free surface elevation is expressed as follows using linear wave theory (LWT):

$$\eta(x,t) = \sum_{i=1}^{n} a_i \cos(k_i x - \omega_i + \varphi_i) \tag{1}$$

Here, x represents the distance to the mean wave-maker position, t represents the time, a_i is the wave amplitude of the ith component, k_i is the wave number, ω_i is the wave angular frequency, and ϕ_i is the phase angle at the focusing point.

The input parameters of Eq.(1) are the steepness, the wave spectrum type, the phase at focusing, the focus location, and the peak frequency (f_p). The focus of a wave train is mainly due to dispersion (Eq.(2)).

$$(2\pi f_s)^2 = g\ k_s \tanh(k_s h_0) \tag{2}$$

where k_s represents the characteristic wavenumber and f_s represents the characteristic frequency.

The initial local wave steepness (S_0) for characterizing the nonlinearity of the wave train is determined from the free surface elevation obtained by the resistive probe placed 4 meters from the wave-maker. We consider that the wave train is well-formed by this point. The parameter was calculated using the formula (Eq.(3)), see [6], [19] and [23]:

$$S_0 = k_{S0} \sum_{i=1}^{n} a_i \tag{3}$$

where k_{S0} is the spectrally weighted wave number calculated using the dispersion relation at x = -5.6 m and $\sum a_i$ represents the surface elevation at the focal point according to LWT.

The wave trains generated are based on a Pierson-Moskowitz (Eq.(4)) [24] or a JONSWAP (Eq.(5)) spectrum [25]. The Pierson-Moskowitz spectrum is often used to describe the sea state in shallow water. It can be described by the following:

$$E_{pm}(f) = \alpha \frac{g^2}{(2\pi)^4}\ f^{-5} exp[-1.25\ (\frac{f}{f_p})^{-4}] \tag{4}$$

with α = 0.0081: Philips constant determined empirically; $f_p = \frac{g v_{19.5}^{PM}}{U_{19.5}}$: peak frequency where $v_{19.5}^{PM}$=0.14 and $U_{19.5}$ represents the wind speed on the fetch at 19.5 m of the free surface.

A correction factor was added to the Pierson-Moskowitz spectrum, the peak enhancement factor γ, to improve the prediction of the energy spectral density of sea states. Therefore, the JONSWAP spectrum (Joint North Sea Wave Project) is defined by the following:

$$E_J(f) = \alpha \frac{g^2}{(2\pi)^4} f^{-5} exp[-1.25 (\frac{f}{f_p})^{-4}] \gamma^{\delta} \quad (5)$$

With $\alpha = (\frac{gF}{U_{10}^2})^{-0.22}$; $\delta = exp(\frac{-(\frac{f}{f_p}-1)^2}{2\sigma^2})$ et $\sigma = 0.07$ if $f \leq f_p$ et 0.09 if $f > f_p$

The peak enhancement factor γ determines the height of the peak and the narrowness of the spectrum. For practical purposes, it usually ranges from 1 for a Pierson-Moskowitz spectrum to 7 for the narrowest spectrum.

Table 1. Table showing the parameters used.

Spectrum	PIERSON-MOSKOWITZ	JONSWAP (γ = 3.3)	JONSWAP (γ = 7)
Peak frequency f_p	0.75 Hz	0.75 Hz	0.75 Hz
Non-linearity S_0	0.19	0.21	0.21
	0.24	0.26	0.27
	0.29	0.31	0.34
	0.35	0.38	0.41
	0.40	0.44	0.49
	0.46	0.51	0.58
	0.52	0.58	0.65
	0.58	0.66	0.70
	0.65	0.74	0.72
Number of Trains	1 – 3 – 6 – 9	1 – 3 – 6 – 9	1 – 3 – 6 – 9
WG positions	51	51	51

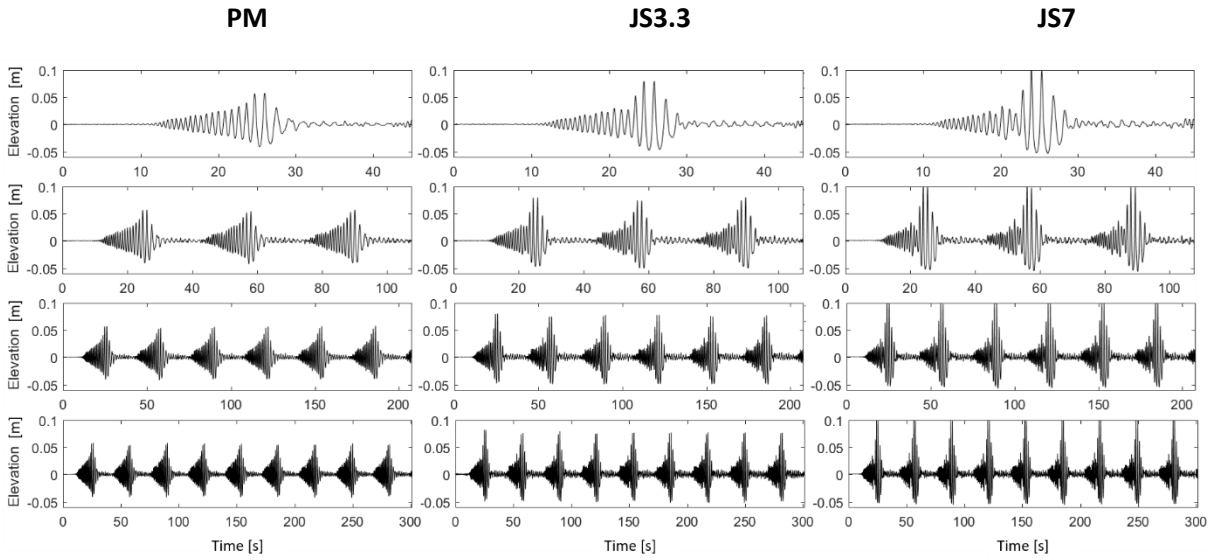

Figure 2. Reference wave gauge (WG_R) signals for three different spectra, namely Pierson-Moskowitz, JONSWAP (γ=3.3), and JONSWAP (γ=7), using one, three, six, and nine wave trains.

3. Wave Energy

3.1. Power spectral density

Spectral analysis provides the dissection of temporal signals into their component frequencies. This method is especially advantageous for comprehending fast time-varying phenomena like waves. It can be utilized to establish features such as dominant frequencies, harmonic content, periodicity and quantify the energy dissipation during wave propagation. (see [6], [7], [19]). The measured signals were low-pass filtered to eliminate the spurious high-frequency band that could be contaminated by the electronic noise from the wave probes. The spectra were estimated using Welch's method. A 50% overlap was employed to divide the signals into multiple segments. Each segment of the signal (approximately 16s) was first subjected to the Hann window before undergoing a 2^{10}-point fast Fourier transform (FFT), which produced a high spectral resolution of Δf = 0.03125 Hz.

The spatial evolution of the spectrum as well as the detailed spectra at three specific positions are provided in Figures 3 and 4 using the same nonlinearity S_0 = 0.65. These positions were (x = -5.6 m, x = 2 m, and x = 3.8 m, where 0 is the toe of the slope) corresponding to WG1 representing the

initial wave signal, WG39 describing the signal before wave breaking, and finally WG48 as the last position, respectively. Two scenarios were examined, a single wave train signal (Figure 3) and a nine wave trains signal (Figure 4).

On the first hand, it was observed that the Pierson-Moskowitz spectrum has a wider and less concentrated energy distribution with a peak frequency f_p = 0.75 Hz (Figure 3a). On the other hand, the JONSWAP 3.3 spectrum has a narrower energy distribution with a distinct peak f_p (Figure 3c). Moreover, the JONSWAP 7 spectrum accentuates energy concentration at the peak frequency due to its higher γ value (Figure 3e).

Figure 3 shows that the spectrum of waves undergoes a widening process as the wave propagates towards the shore. The dissipation process leads to a decrease in the total spectral energy of the waves. This remarkable evolution of the wave spectrum is influenced by a combination of two critical elements, boundary friction and the nonlinear wave interactions. The three spectrograms show that the energy is focused at the peak frequency f_p = 0.75 Hz and dissipates strongly after the wave breaking which occurs around x = 2m.

The JONSWAP spectrum more accurately represents energy dissipation due to wave breaking than the Pierson-Moskowitz spectrum [26]. This is demonstrated by comparing WG39 and WG48 for all three spectra. When using the Pierson-Moskowitz spectrum (Figure 3b), the wave breaking that occurred just after WG39 did not show much difference between WG39 and WG48. However, when using the JONSWAP (γ=7) spectrum (Figure 3f), the difference is more noticeable.

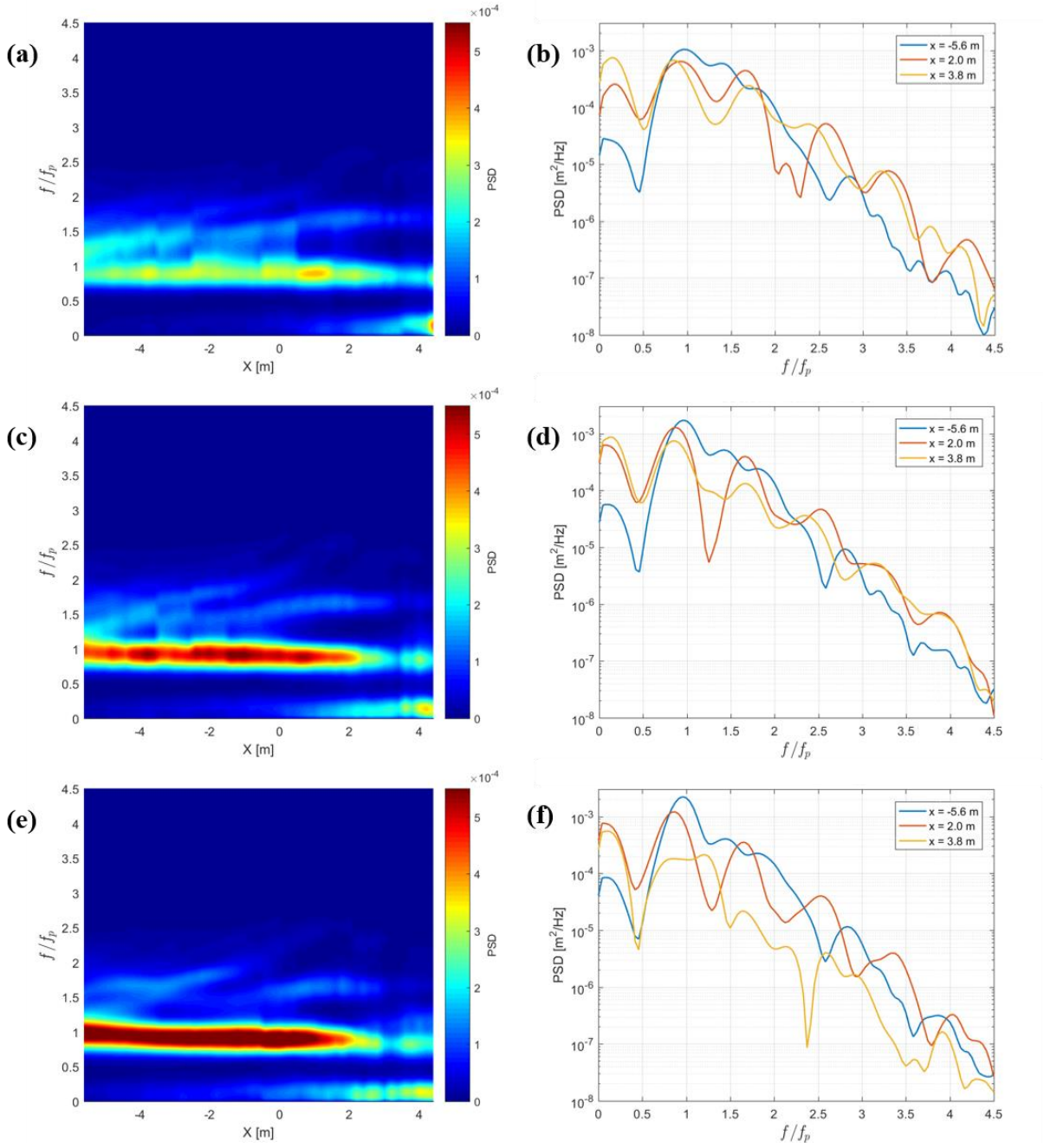

Figure 3. Spatial evolution of the spectrum and Spectra of three positions using a signal of one wave train and S_0 = 0.65 for: (a), (b) Pierson-Moskowitz (γ =1) spectrum; (c), (d) JONSWAP (γ=3.3) spectrum; and (e), (f) JONSWAP (γ=7) spectrum, respectively.

Figure 4 shows that the multi-wave train signal exhibits notably higher energy levels compared to the single-wave train signal (Figure 3) within the spatial range of x ∈ [-5.6 m, 2 m]. This distinction

is evident, for example, by comparing Figure 3a and Figure 4a. The marked energy difference highlights the impact of the multi-wave train configuration on the overall spectral properties.

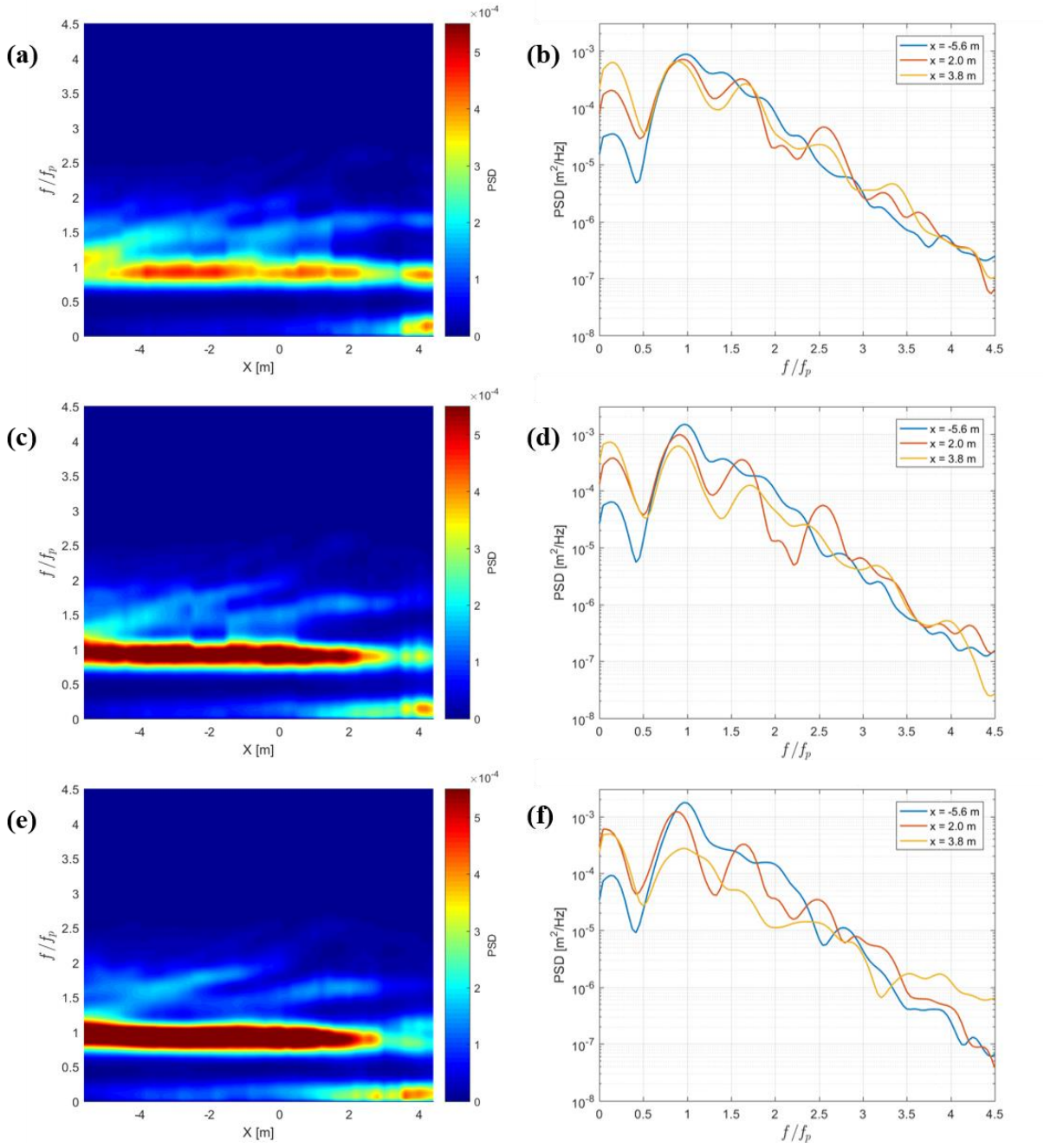

Figure 4. Spatial evolution of the spectrum and Spectra of three positions using a signal of nine wave trains and S_0 = 0.65 for: (a), (b) Pierson-Moskowitz (γ =1) spectrum; (c), (d) JONSWAP (γ=3.3) spectrum; and (e), (f) JONSWAP (γ=7) spectrum, respectively.

3.2. Energy Dissipation

For each frequency, the energy spectral density $S(f)$ can be calculated (Eq.(6)), which represents the contribution of waves to the energy at that specific frequency. By adding up the energy across all frequencies, the total wave energy (S) can be determined (Eq.(7)).

$$S(f) = 2|F(f)|^2 \tag{6}$$

When calculating S, only the Fourier components within the interval [f_1, f_2] are taken into account. The two frequencies, $f_1 = f_{min} = 0.2\ Hz$ and $f_2 = f_{max} = 3f_p\ Hz$ are referred to as the cutoff frequencies, and the spectral density is considered negligible elsewhere.

$$S = \sum_{f_1}^{f_2} S(f) \tag{7}$$

The wave energy along the flume was calculated. The energy dissipation E_D percentage is then derived by calculating the differential between two consecutive wave gauge positions using:

$$Energy\ Dissipation\ (E_D)\ \% = \frac{S_{WG(i)} - S_{WG(i-1)}}{S_{WG(i)}} \times 100 \tag{8}$$

Energy dissipation percentage using a signal of one and nine wave trains is shown in Figure 5 and Figure 6, respectively. Pierson-Moskowitz, JONSWAP (γ = 3.3), and JONSWAP (γ = 7) spectra are investigated in these figures with a nonlinearity $S_0 \in [0.4, 0.65]$. It can be seen that for a range of $x \in$ [-5.6m, 2m], there is a reduction in wave energy. These losses are caused by viscose boundary layers at the sidewalls and bottom, dissipation in the boundary layer at the free surface, in the bulk of the water, and contact-line damping. Furthermore, wave breaking, which takes place around 2m from the slope's toe, has a notable impact on energy dissipation. It can be concluded that the variation in the wave spectrum before and after breaking, as seen in Figure 3 and Figure 4, is due to the energy dissipation caused by the wave breaking.

Wave nonlinearity S_0 has a significant effect on wave energy dissipation, as depicted in Figure 5 and Figure 6, showing an increasing percentage of dissipation with S_0. For instance, in the wave-breaking area $x \in$ [2 m, 3 m], the dissipation percentage has risen from approximately 5% for S_0 = 0.4 to 13% for S_0 = 0.65. It is noticed that the dissipation of the wave train increases again as the low-frequency waves shoal closer to the coast (x > 4 m).

It can also be seen that as the peak enhancement factor γ is increased from 1 for the Pierson-Moskowitz spectrum to 3.3 and 7 for the JONSWAP spectrum, the energy dissipation becomes more significant. The value of γ determines the extent to which the energy is concentrated around the peak frequency, producing a more nonlinear spectrum with a more pronounced peak. This concentration of energy around the peak wave can result in more intense wave events and potentially more energy dissipation.

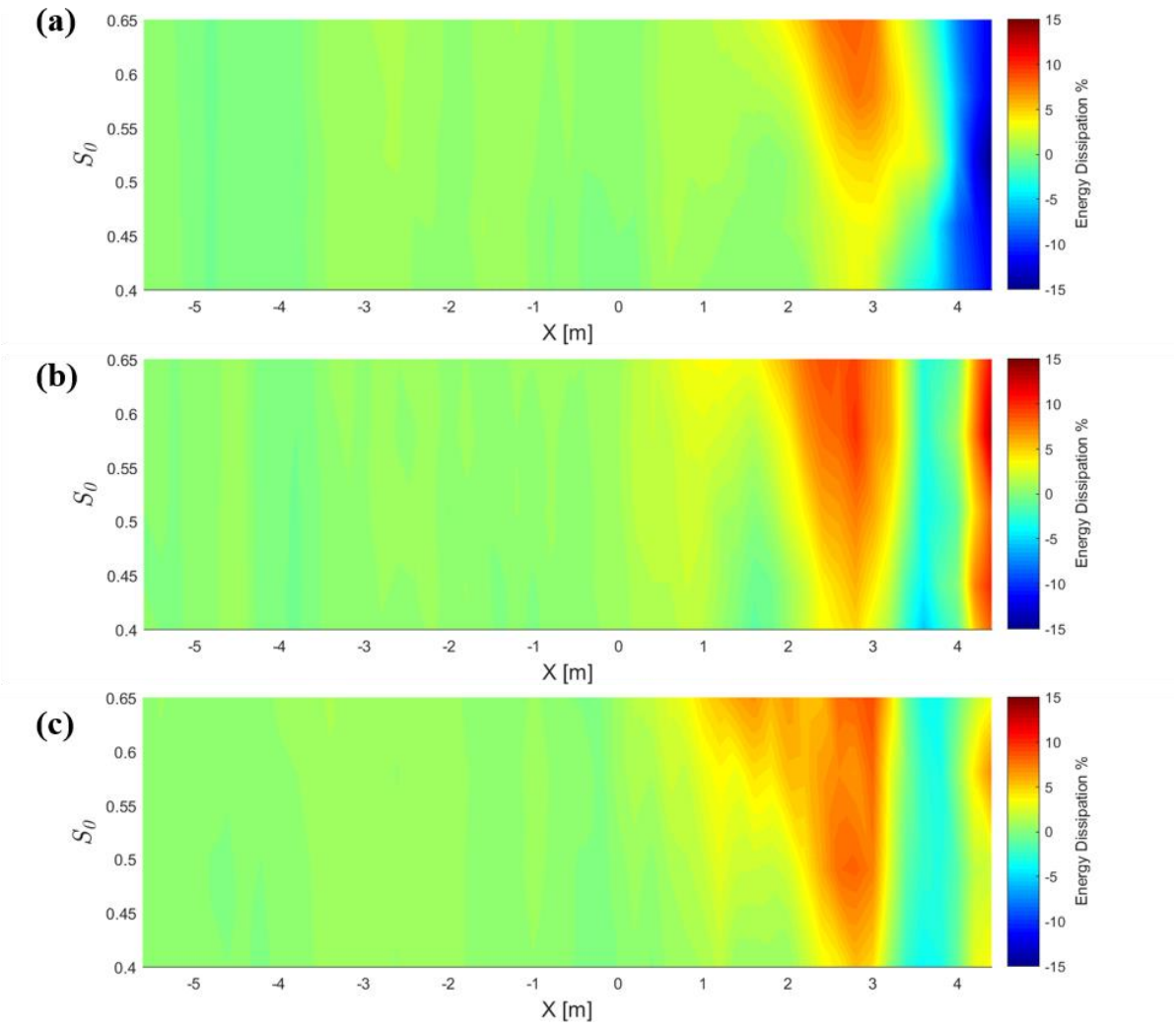

Figure 5. Energy dissipation percentage using a signal of one wave train and several nonlinearities for: (a) Pierson-Moskowitz (γ =1) spectrum, (b) JONSWAP (γ=3.3) spectrum, and (c) JONSWAP (γ=7) spectrum.

In our investigation of energy dissipation, we examined both single and nine-wave trains signals (Figure 5 and Figure 6 respectively). It seems that the energy dissipation is more concentrated

around the wave breaking area for the multi-wave train signal case. For instance, the dissipation observed for $x \in [2\text{ m}, 3\text{ m}]$ in Figure 6c is significantly more concentrated than in Figure 5c. Our results indicate that the duration of the extreme events not only impacts spectral energy but also plays a significant role in shaping the spatial distribution of energy dissipation.

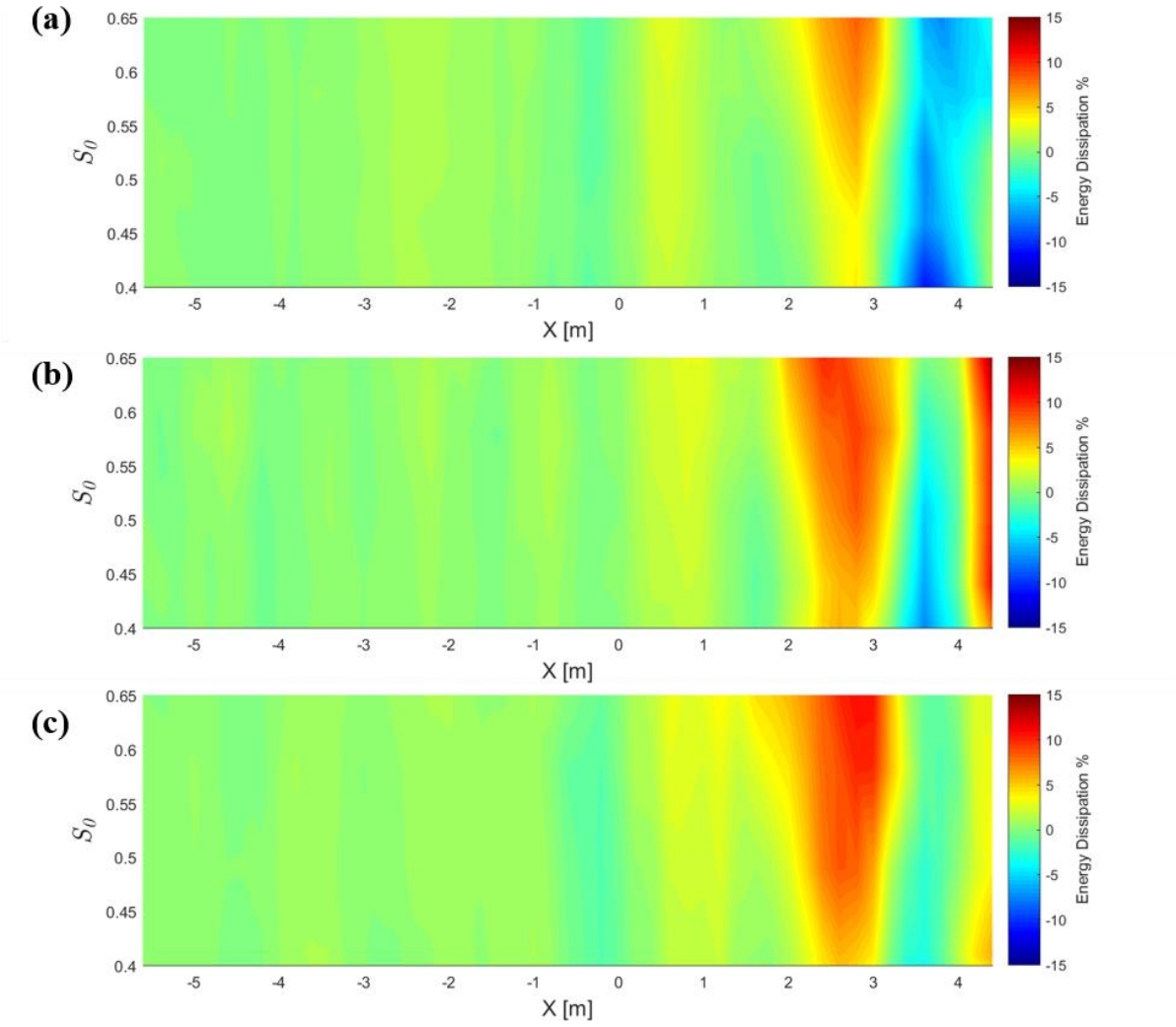

Figure 6. Energy dissipation percentage using a signal of nine wave trains and several nonlinearities for: (a) Pierson-Moskowitz (γ =1) spectrum, (b) JONSWAP (γ=3.3) spectrum, and (c) JONSWAP (γ=7) spectrum.

4. Frequency components and wavelet analysis

The Linear Wave Theory (LWT), which assumes non-interaction among frequency components in a given sea state, falls short of adequately describing the physics of wave train propagation. This

is because intense energy transfers occur at the propagation site between different frequency components. The wavelet transform technique offers time-frequency localization and is therefore a more suitable approach. The Discrete wavelet transform (DWT) is recommended for decomposing hydrological time series data [27], [28]. However it is important to note that the DWT is sensitive to the length of the time series [29]. To overcome this, the maximal overlap DWT (MODWT) was implemented in this study [30], [31]. It is particularly suitable for handling non-stationary and irregularly sampled data using overlapping segments. The MODWT algorithm decomposes the signal into various scale levels, arranged from high to low frequencies while keeping the amplitudes of the transform aligned with the amplitude in the original signal [17]. This decomposition consists of applying a sequence of low-pass and high-pass filters capable of producing the spectral components that describe the entire signal [32]. For more details see [17], [18].

The MODWT method was used to decompose the reference wave gauge signal WG_R (Figure 7). Figure 8 shows the decomposed components (d) ranging from d1, corresponding to the higher frequency, to d9, corresponding to the lowest frequency. The red-framed d5 and d4 components are dominant and correspond to the peak frequency (f_p = 0.75 Hz) and its first harmonic ($2f_p$ = 1.5 Hz). Furthermore, the percentage of energy that each spectral component contributes to the total variability is estimated, indicating the importance of each detail [31]. Figure 9 illustrates the spatial evolution of the decomposed components (d1 – d9) energy along the wave flume using a JONSWAP (γ=3.3) signal of nine wave trains and a nonlinearity S_0 = 0.66. Note that at each position, the total contribution of all frequency components adds up to 100 %.

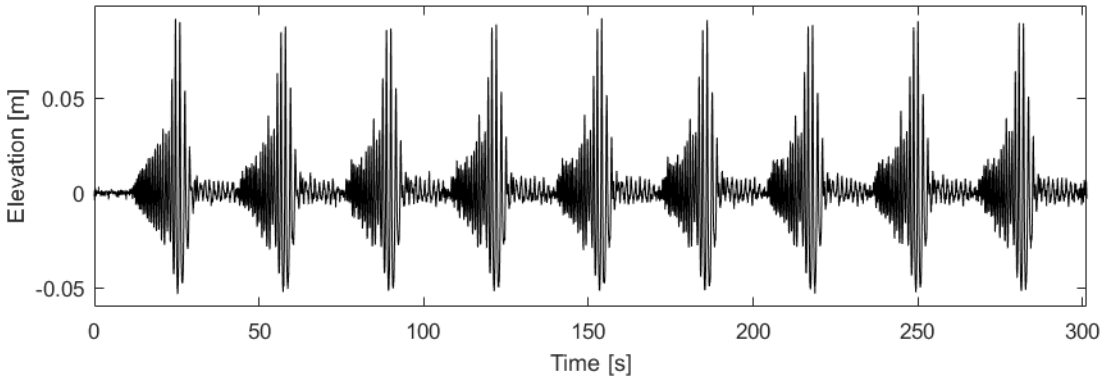

Figure 7. Free surface elevation of the reference wave gauge WG_R using a JONSWAP (γ=3.3) signal of nine wave trains and S_0 = 0.66.

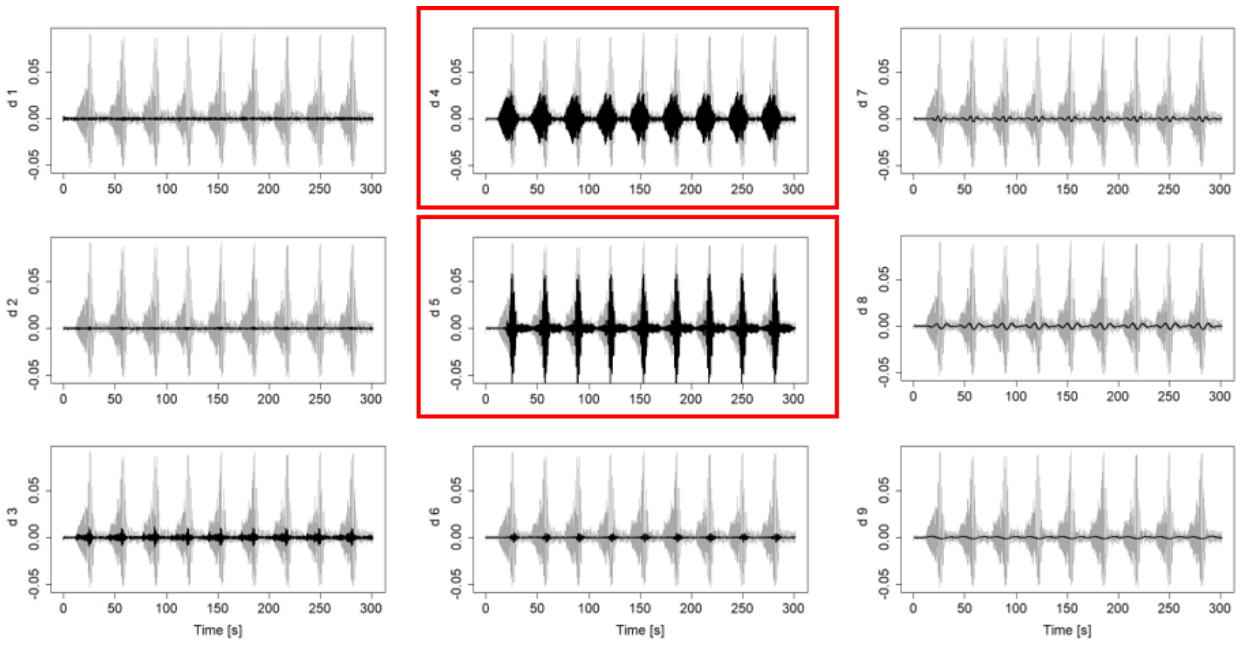

Figure 8. Frequency components of the reference signal ranging from d1 to d9, with the dominant components being d5 (the peak frequency) and d4 (harmonic frequency).

Components d5 and d4, which correspond to the peak frequency and its first harmonic, experience a decrease in energy while the other components exhibit an increase (Figure 9). For example, d4 and d5 each experienced a 15 % and 30 % reduction in energy, respectively, while d8 (f = 0.094 Hz), which had initially been insignificant, had increased to an energy value of 20 % by the end of the testing zone. It is assumed that the energy lost by d4 and d5 is recovered by the other components. This finding aligns with the result reported in [33], suggesting that wave components at frequencies significantly below or near the peak frequency can gain a small portion of the energy lost by high-frequency waves.

To further examine this evolution of frequency components energy, the energy differential ($S_{WG(i)} - S_{WG(i-1)}$) was calculated to reveal the zones of higher energy exchange using various nonlinearities (see Figure 10). Six frequency components significantly exchanging energy were selected (d4 – d9). It should be noted that in the case of the d4 and d5 components, the absolute value of the difference is taken into account to maintain the coherence of all figures. This energy exchange becomes particularly significant at the beginning of the wave breaking at x = 2m and increases as the nonlinearity increases (Figure 10).

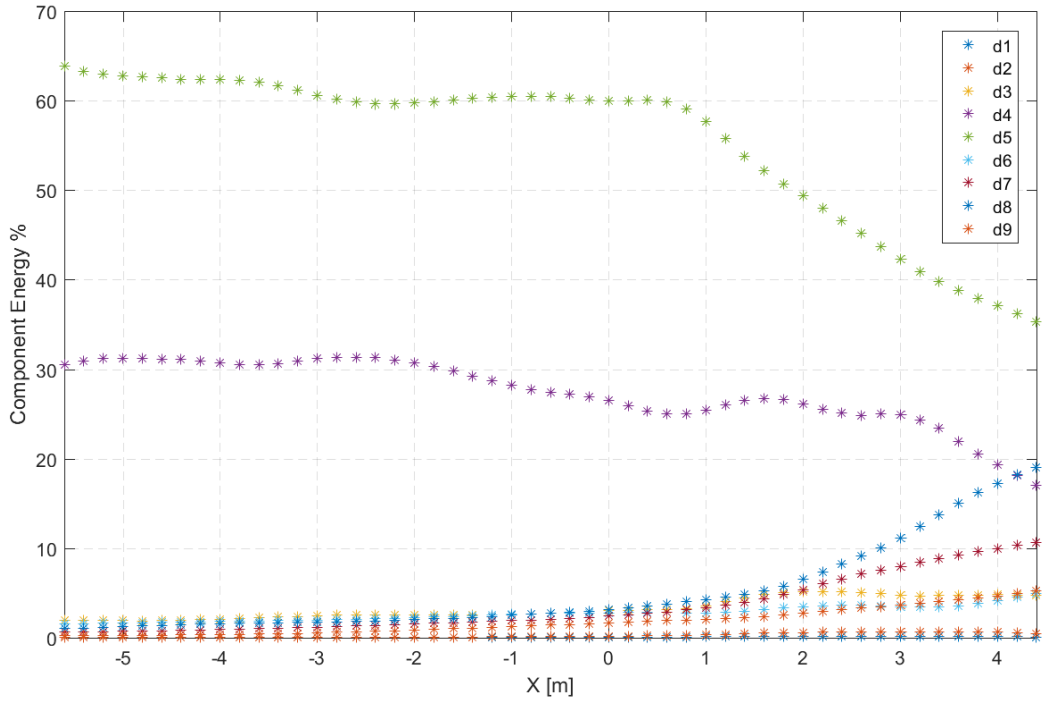

Figure 9. Spatial evolution of frequency components energy using a JONSWAP (γ=3.3) signal of nine wave trains and S_0 = 0.66.

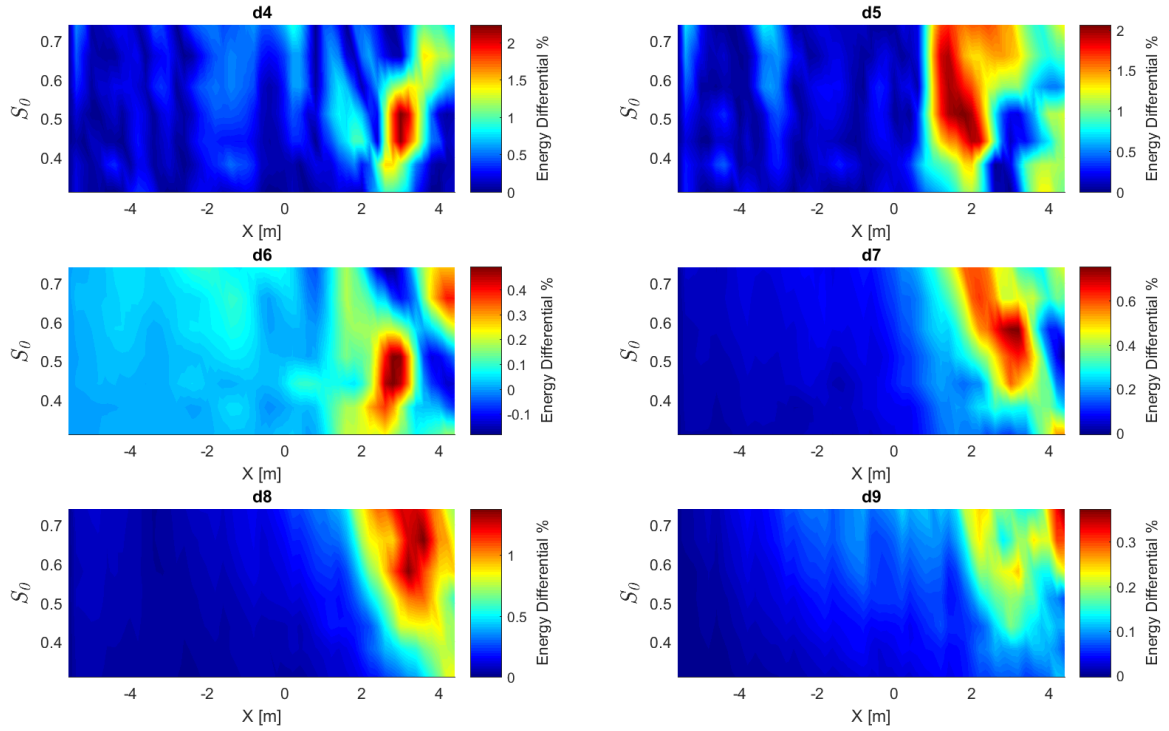

Figure 10. Spatial evolution of six frequency components (d4-d9) energy differential using a JONSWAP (γ=3.3) signal of nine wave trains and several nonlinearities.

5. Discussion and Conclusions

When non-linear waves with sufficient energy encounter each other, they can interact in various ways. Energy dissipation occurs during non-linear wave-wave interactions, especially in cases of wave breaking, where the wave's energy is transformed into turbulent kinetic energy and heat due to the chaotic motion of water particles. It was observed that this energy dissipation has increased with the nonlinearity $S_{0.}$ Moreover, the multi-wave train signal investigated in this study showed significantly higher energy levels and a more focused energy dissipation around the wave breaking area ($x \in [2, 3]$) when compared to the single-wave train signal. This observation underscores that the duration of extreme events plays a crucial role in shaping the spatial distribution of energy dissipation. The Wavelet Transform Analysis using the MODWT method provided an additional level of comprehension by identifying particular frequency components related to the process of energy dissipation. This comprehensive frequency decomposition enabled a subtler understanding of the individual contributions of different components of the wave spectrum to dissipation. Based on the wavelet transform analysis, during these non-linear interactions, energy can be transferred between different frequency components.

Furthermore, rapid advances in wave forecasting have made machine learning (ML) a valuable tool, providing a wealth of techniques for extracting information from data [34]–[36]. The Multilayer Perceptron (MLP) algorithm [37], [38], is selected from several machine learning algorithms for its applicability to complex nonlinear problems and its ability to handle large input data sets [39]. It is used to verify the repetitive and accurate nature of our results in forecasting the spatial evolution of frequency component energy. MLP-Regressor is a supervised learning technique that effectively processes information through nonlinear regression by optimizing the squared error. This robust algorithm has already shown its usefulness for various applications [40], [41]. The MLP-Regressor input data sets included wave spectrum, wave nonlinearity, abscissa along the flume, water height, and energy values of frequency components (d1-d9). The programming environment is based on the Python library Scikit-Learn version 0.21.3. Figure 11 shows a simplified schematic diagram of the Multilayer Perceptron algorithm (MLP). Our predictions adequately coincide with the data. The predictions of two specific frequency components are selected in the following, d5 (Figure 12a) and d8 (Figure 12b), which exhibited distinguishable variation in Figure 9.

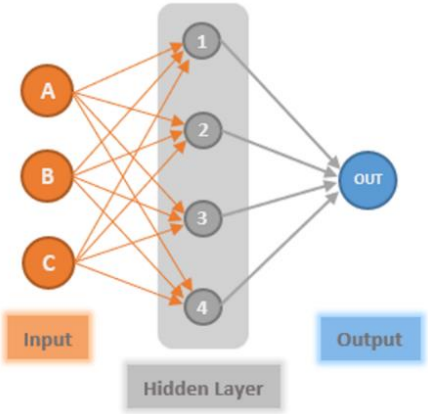

Figure 11. A simplified schematic diagram of the Multilayer Perceptron Model (MLP) showing the input, hidden, and output layers.

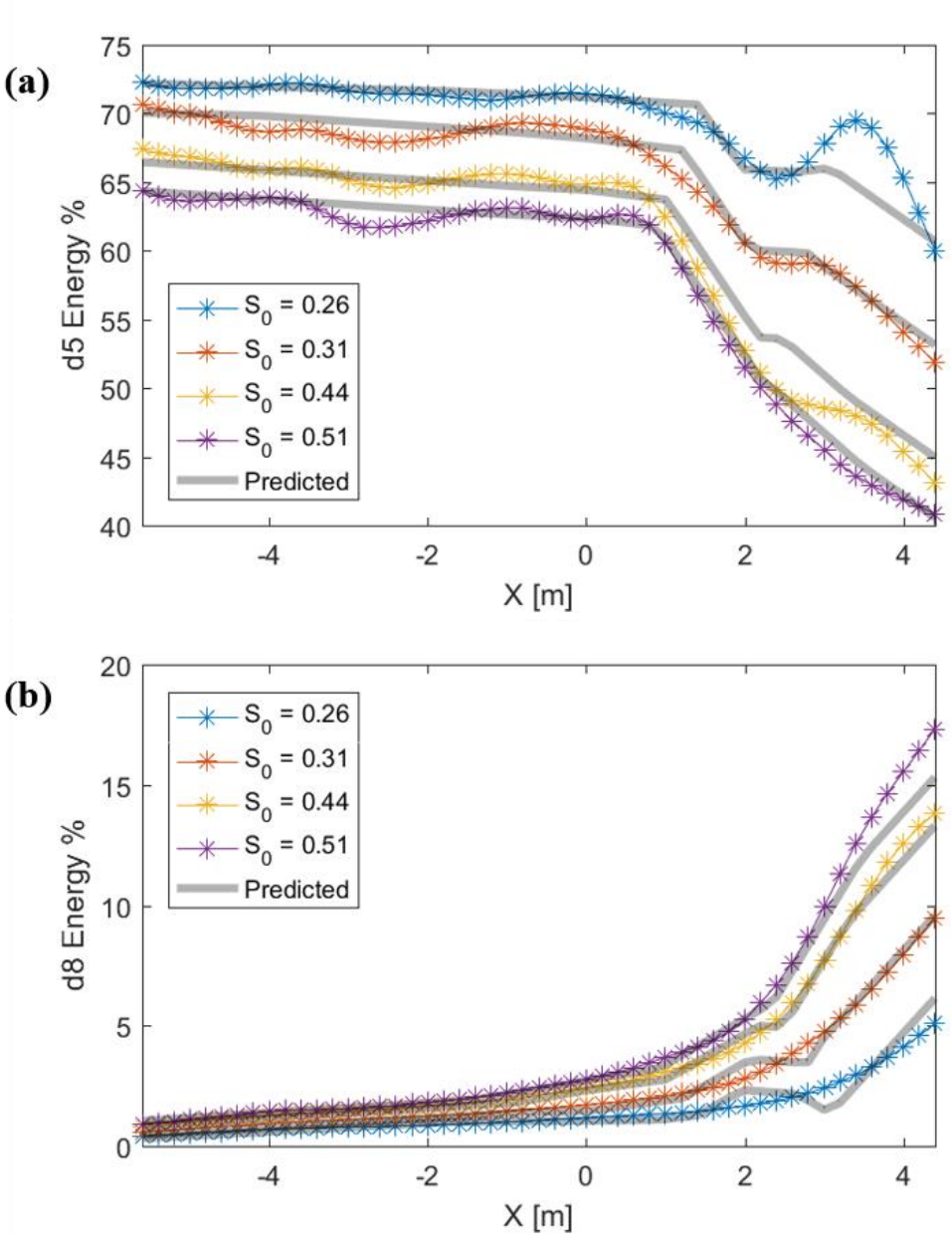

Figure 12. The spatial evolution of a) d5 and b) d8 for a JONSWAP (γ=3.3) signal of nine wave trains using several nonlinearities. The experimental results are represented by dotted curves, while the predicted results are shown by the grey continuous line.

The predicted values in grey, along with the dotted curves obtained experimentally, overlap with an accuracy of 98%. This work illustrates the effectiveness of the MLP algorithm in enhancing wave prediction based on field experimental data. In the near future, we plan to investigate how environmental factors, such as, water depth, and seabed composition, influence the observed

interactions. Understanding environmental dependencies can enhance the predictive capability of models and contribute to site-specific wave energy management strategies.

References

[1] L. Erikson *et al.*, "Global ocean wave fields show consistent regional trends between 1980 and 2014 in a multi-product ensemble," *Commun Earth Environ*, vol. 3, no. 1, p. 320, Dec. 2022, doi: 10.1038/s43247-022-00654-9.

[2] W. Sweet *et al.*, "Global and regional sea level rise scenarios for the United States," Report, 2022. [Online]. Available: https://pubs.usgs.gov/publication/70229139

[3] M. V. Martello and A. J. Whittle, "Estimating coastal flood damage costs to transit infrastructure under future sea level rise," *Commun Earth Environ*, vol. 4, no. 1, p. 137, Apr. 2023, doi: 10.1038/s43247-023-00804-7.

[4] M. Oppenheimer and R. B. Alley, "How high will the seas rise?," *Science*, vol. 354, no. 6318, pp. 1375–1377, Dec. 2016, doi: 10.1126/science.aak9460.

[5] P. Petrova and C. Guedes Soares, "Maximum wave crest and height statistics of irregular and abnormal waves in an offshore basin," *Applied Ocean Research*, vol. 30, no. 2, pp. 144–152, Apr. 2008, doi: 10.1016/j.apor.2008.08.004.

[6] I. Abroug, N. Abcha, D. Dutykh, A. Jarno, and F. Marin, "Experimental and numerical study of the propagation of focused wave groups in the nearshore zone," *Physics Letters A*, vol. 384, no. 6, p. 126144, Feb. 2020, doi: 10.1016/j.physleta.2019.126144.

[7] I. Abroug, N. Abcha, A. Jarno, and F. Marin, "Laboratory study of non-linear wave–wave interactions of extreme focused waves in the nearshore zone," *Nat. Hazards Earth Syst. Sci.*, vol. 20, no. 12, pp. 3279–3291, Dec. 2020, doi: 10.5194/nhess-20-3279-2020.

[8] M. Onorato, S. Residori, U. Bortolozzo, A. Montina, and F. T. Arecchi, "Rogue waves and their generating mechanisms in different physical contexts," *Physics Reports*, vol. 528, no. 2, pp. 47–89, Jul. 2013, doi: 10.1016/j.physrep.2013.03.001.

[9] C. Kharif and E. Pelinovsky, "Physical mechanisms of the rogue wave phenomenon," *European Journal of Mechanics - B/Fluids*, vol. 22, no. 6, pp. 603–634, Nov. 2003, doi: 10.1016/j.euromechflu.2003.09.002.

[10] C. N. Whittaker, C. J. Fitzgerald, A. C. Raby, P. H. Taylor, and A. G. L. Borthwick, "Extreme coastal responses using focused wave groups: Overtopping and horizontal forces exerted on an inclined seawall," *Coastal Engineering*, vol. 140, pp. 292–305, Oct. 2018, doi: 10.1016/j.coastaleng.2018.08.004.

[11] K. Dysthe, H. E. Krogstad, and P. Müller, "Oceanic Rogue Waves," *Annu. Rev. Fluid Mech.*, vol. 40, no. 1, pp. 287–310, Jan. 2008, doi: 10.1146/annurev.fluid.40.111406.102203.

[12] J. Zhang, M. Benoit, O. Kimmoun, A. Chabchoub, and H.-C. Hsu, "Statistics of Extreme Waves in Coastal Waters: Large Scale Experiments and Advanced Numerical Simulations," *Fluids*, vol. 4, no. 2, p. 99, May 2019, doi: 10.3390/fluids4020099.

[13] K. Trulsen, H. Zeng, and O. Gramstad, "Laboratory evidence of freak waves provoked by non-uniform bathymetry," *Physics of Fluids*, vol. 24, no. 9, p. 097101, Sep. 2012, doi: 10.1063/1.4748346.

[14] H. Kashima, K. Hirayama, and N. Mori, “ESTIMATION OF FREAK WAVE OCCURRENCE FROM DEEP TO SHALLOW WATER REGIONS,” *Int. Conf. Coastal. Eng.*, vol. 1, no. 34, p. 36, Oct. 2014, doi: 10.9753/icce.v34.waves.36.
[15] S. R. Massel, “Wavelet analysis for processing of ocean surface wave records,” *Ocean Engineering*, vol. 28, no. 8, pp. 957–987, Aug. 2001, doi: 10.1016/S0029-8018(00)00044-5.
[16] R. Fu, Y. Ma, G. Dong, and M. Perlin, “A wavelet-based wave group detector and predictor of extreme events over unidirectional sloping bathymetry,” *Ocean Engineering*, vol. 229, p. 108936, Jun. 2021, doi: 10.1016/j.oceaneng.2021.108936.
[17] D. B. Percival and A. T. Walden, *Wavelet Methods for Time SeriesAnalysis*. Cambridge: Cambridge University Press, 2000. doi: 10.1017/CBO9780511841040.
[18] C. R. Cornish, C. S. Bretherton, and D. B. Percival, “Maximal Overlap Wavelet Statistical Analysis With Application to Atmospheric Turbulence,” *Boundary-Layer Meteorol*, vol. 119, no. 2, pp. 339–374, May 2006, doi: 10.1007/s10546-005-9011-y.
[19] I. Abroug, R. Matar, and N. Abcha, “Spatial Evolution of Skewness and Kurtosis of Unidirectional Extreme Waves Propagating over a Sloping Beach,” *JMSE*, vol. 10, no. 10, p. 1475, Oct. 2022, doi: 10.3390/jmse10101475.
[20] J. Xu, S. Liu, J. Li, and W. Jia, “Experimental study of wave height, crest, and trough distributions of directional irregular waves on a slope,” *Ocean Engineering*, vol. 242, p. 110136, Dec. 2021, doi: 10.1016/j.oceaneng.2021.110136.
[21] T. A. A. Adcock and P. H. Taylor, “Estimating ocean wave directional spreading from an Eulerian surface elevation time history,” *Proc. R. Soc. A.*, vol. 465, no. 2111, pp. 3361–3381, Nov. 2009, doi: 10.1098/rspa.2009.0031.
[22] P. Tromans, A. R. Anaturk, and P. Hagemeijer, “A new model for the kinematics of large ocean waves-application as a design wave,” *Proc. ISOPE-91*, vol. 3, Jan. 1991.
[23] Z. Tian, M. Perlin, and W. Choi, “Energy dissipation in two-dimensional unsteady plunging breakers and an eddy viscosity model,” *J. Fluid Mech.*, vol. 655, pp. 217–257, Jul. 2010, doi: 10.1017/S0022112010000832.
[24] W. J. Pierson and L. Moskowitz, “A proposed spectral form for fully developed wind seas based on the similarity theory of S. A. Kitaigorodskii,” *J. Geophys. Res.*, vol. 69, no. 24, pp. 5181–5190, Dec. 1964, doi: 10.1029/JZ069i024p05181.
[25] K. Hasselmann *et al.*, “Measurements of wind-wave growth and swell decay during the Joint North Sea Wave Project (JONSWAP),” *Deut. Hydrogr. Z.*, vol. 8, pp. 1–95, Jan. 1973.
[26] C. C. Craciunescu and M. Christou, “Wave breaking energy dissipation in long-crested focused wave groups based on JONSWAP spectra,” *Applied Ocean Research*, vol. 99, p. 102144, Jun. 2020, doi: 10.1016/j.apor.2020.102144.
[27] M. Rezaie-balf, S. R. Naganna, A. Ghaemi, and P. C. Deka, “Wavelet coupled MARS and M5 Model Tree approaches for groundwater level forecasting,” *Journal of Hydrology*, vol. 553, pp. 356–373, Oct. 2017, doi: 10.1016/j.jhydrol.2017.08.006.
[28] S. Mouatadid, J. F. Adamowski, M. K. Tiwari, and J. M. Quilty, “Coupling the maximum overlap discrete wavelet transform and long short-term memory networks for irrigation flow forecasting,” *Agricultural Water Management*, vol. 219, pp. 72–85, Jun. 2019, doi: 10.1016/j.agwat.2019.03.045.
[29] J. Quilty and J. Adamowski, “Addressing the incorrect usage of wavelet-based hydrological and water resources forecasting models for real-world applications with best practices and a

new forecasting framework," *Journal of Hydrology*, vol. 563, pp. 336–353, Aug. 2018, doi: 10.1016/j.jhydrol.2018.05.003.

[30] N. Massei *et al.*, "Multi-time-scale hydroclimate dynamics of a regional watershed and links to large-scale atmospheric circulation: Application to the Seine river catchment, France," *Journal of Hydrology*, vol. 546, pp. 262–275, Mar. 2017, doi: 10.1016/j.jhydrol.2017.01.008.

[31] E. I. Turki *et al.*, "Multi-timescale dynamics of extreme river flood and storm surge interactions in relation with large-scale atmospheric circulation: Case of the Seine estuary," *Estuarine, Coastal and Shelf Science*, vol. 287, p. 108349, Jul. 2023, doi: 10.1016/j.ecss.2023.108349.

[32] A. T. M. S. Rahman, T. Hosono, J. M. Quilty, J. Das, and A. Basak, "Multiscale groundwater level forecasting: Coupling new machine learning approaches with wavelet transforms," *Advances in Water Resources*, vol. 141, p. 103595, Jul. 2020, doi: 10.1016/j.advwatres.2020.103595.

[33] S. Zhang, "Energy and momentum dissipation through wave breaking," *J. Geophys. Res.*, vol. 110, no. C9, p. C09021, 2005, doi: 10.1029/2004JC002834.

[34] K. Günaydın, "The estimation of monthly mean significant wave heights by using artificial neural network and regression methods," *Ocean Engineering*, vol. 35, no. 14–15, pp. 1406–1415, Oct. 2008, doi: 10.1016/j.oceaneng.2008.07.008.

[35] I. Malekmohamadi, M. R. Bazargan-Lari, R. Kerachian, M. R. Nikoo, and M. Fallahnia, "Evaluating the efficacy of SVMs, BNs, ANNs and ANFIS in wave height prediction," *Ocean Engineering*, vol. 38, no. 2–3, pp. 487–497, Feb. 2011, doi: 10.1016/j.oceaneng.2010.11.020.

[36] S. C. James, Y. Zhang, and F. O'Donncha, "A machine learning framework to forecast wave conditions," *Coastal Engineering*, vol. 137, pp. 1–10, Jul. 2018, doi: 10.1016/j.coastaleng.2018.03.004.

[37] J. Rynkiewicz, "General bound of overfitting for MLP regression models," *Neurocomputing*, vol. 90, pp. 106–110, Aug. 2012, doi: 10.1016/j.neucom.2011.11.028.

[38] H. White, *Artificial Neural Networks: Approximation and Learning Theory*. USA: Blackwell Publishers, Inc., 1992.

[39] B. Akkaya and N. Çolakoğlu, "Comparison of Multi-class Classification Algorithms on Early Diagnosis of Heart Diseases," Sep. 2019.

[40] Y. Qin, C. Li, X. Shi, and W. Wang, "MLP-Based Regression Prediction Model For Compound Bioactivity," *Front. Bioeng. Biotechnol.*, vol. 10, p. 946329, Jul. 2022, doi: 10.3389/fbioe.2022.946329.

[41] J. Maqbool, P. Aggarwal, R. Kaur, A. Mittal, and I. A. Ganaie, "Stock Prediction by Integrating Sentiment Scores of Financial News and MLP-Regressor: A Machine Learning Approach," *Procedia Computer Science*, vol. 218, pp. 1067–1078, 2023, doi: 10.1016/j.procs.2023.01.086.

Declaration of interests

☒The authors declare that they have no known competing financial interests or personal relationships that could have appeared to influence the work reported in this paper.

☐The authors declare the following financial interests/personal relationships which may be considered as potential competing interests: